Optical Characterization of Deep-Space Object Rotation States

Doyle Hall[1] and Paul Kervin[2]

[1]*Boeing LTS, Kihei, Maui, HI and Colorado Springs, CO*
[2]*Air Force Research Laboratory, Kihei, Maui, HI*

1 SUMMARY

Analysis of time-series data can yield remarkably accurate estimates of the frequency of a satellite's brightness modulations. These "apparent" or synodic frequencies can vary in time, differing from the actual rotation rate of the object by an amount that depends on the relative angular motion between the satellite, illuminator, and observer for reflected light measurements (or between the satellite and observer for thermal emission measurements). When detected with sufficient accuracy, such synodic frequency variations can be exploited to characterize an object's rotation state, using an analysis that does not require any *a priori* knowledge of the object's shape. For instance, this *shape-independent* analysis method can be used to derive spin axis orientations and sidereal rotation rates for spinning objects. Remotely determining such rotation parameters can be useful in many circumstances, such as when performing anomaly resolution for satellites that have lost stabilization. Unfortunately, synodic variations cannot be detected by ground-based observers for many objects due to low rates of relative angular motion. This is especially true for non-specular objects in deep-space and geosynchronous orbits. In these cases, deriving spin axis orientations can be accomplished using a *shape-dependent* method that employs a model of the shape and reflectance characteristics of the object. Our analysis indicates that a simple cylinder shape model can suffice to characterize rotation states for upper-stage rocket bodies, although even this relatively simple model requires significantly more computation than the shape-independent approach.

2 INTRODUCTION

Ground-based optical and radar sites routinely acquire resolved images of satellites, yielding a great deal of knowledge about orbiting spacecraft. However, the important population of deep-space satellites often cannot be resolved, because they are too far away or too small. These must be characterized using methods other than imagery. In this regard, temporal photometry (i.e., measurements of whole-object brightness as a function of time) can be very valuable. For instance, satellite rotational motion can be detected and characterized by analyzing periodic brightness variations [1-5]. Temporal brightness patterns can also be exploited to characterize stabilized GEO satellites [5-10]. The objective of this paper is to outline how temporal photometry can be used to characterize non-resolvable object rotation states, focusing on objects well above low-Earth orbit altitudes.

3 OBSERVATIONS OF NON-RESOLVED ROTATING OBJECTS

This analysis focuses on broad-band temporal photometry of Earth-orbiting satellites (i.e., time-series measurements of whole-object brightnesses) measured by silicon-based CCD detectors sensitive to wavelengths in the 0.4 to 1.1 μm range. In this spectral range, reflected sunlight tends to dominate satellite brightnesses, especially for deep-space objects where contributions from earthshine and other sources can be neglected to first order. Upper-stages from rockets that have launched satellites into orbit represent one of the most common types of rotating object in Earth orbit. Extensive observations of such expended rocket-bodies have been conducted. This analysis focuses on analyzing ground-based observations of one type of upper-stage rocket-body: Boeing's Delta-IV Stage-2 (D4S2).

3.1 Delta-IV Stage 2 Upper Stage Rocket-Bodies

Figure 1 shows a rendering of a D4S2 [11], which like many other rocket-bodies, has a roughly cylindrical shape. D4S2s measure roughly 12.2 m in length and 4 m in diameter, and have been used to launch a variety of geosynchronous/geostationary (GEO) satellites as well as several GPS satellites [11, 12]. As of 2014-07-03, the US Air Force's *Space-Track* web-site tabulated orbital elements for eight D4S2s: four for GEO and four for GPS launches [12]. The four used for GEO launches now reside in geostationary transfer orbits (GTO), with eccentricities $e > 0.5$ and mean motions of ~ 2 revs/day. Those used for GPS launches reside in nearly circular orbits ($e < 0.03$) but have similar mean motions [12].

3.2 Raven Telescope Photometry

During the last few months of 2013, photometric observations of several D4S2s were conducted by AFRL's small Raven telescopes located at the Remote Maui Experiment (RME) site [13, 14]. The top panels of Figures 2-4 show representative plots of three of the measured light-curves. All of the measurements show evidence of periodic

brightness variations. The light-curves vary in duration from a few minutes up to an hour or longer. The longer light-curves often show evidence of significant changes in the amplitude of the brightness variations (see Figure 4).

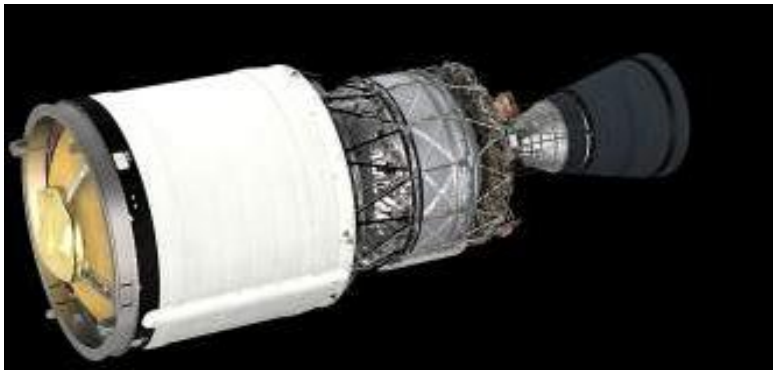

Figure 1. Rendering of the Boeing Delta-IV Stage-2 upper stage rocket-body (from [11]).

3.3 Periodicity and Frequency Spectrum Analysis

The Raven light-curves can be analyzed quantitatively for periodicity using the frequency spectrum and Fourier analysis methods outlined in reference [2]. Figure 5 shows a representative periodicity analysis, in this case for the first ~48 minutes of the SCN 29156 light-curve plotted in Figure 3. The periodicity analysis is a multi-step process. First, a Lomb-Scargle periodogram frequency spectrum [15, 16] is calculated (Figure 5, middle panel), and the peaks in the spectrum above the 99% statistical-significance confidence level identified. Then a peak-by-peak analysis is performed. This analysis subjects the original light-curve data to a polynomial+Fourier series (PFS) fitting process [see 2], in which each peak's best-fit period is refined and then graded according the quality of fit provided. High-quality PFS fits are identified with green symbols on the frequency spectrum, medium-quality fits in yellow, and low-quality in red; the best-fit solution is identified using a triangle and lesser-quality fits using diamonds (Figure 5, middle panel). The final phase "folds" the data, or plots the de-trended brightnesses against the cyclical phase (Figure 5, bottom panel). De-trending entails subtracting the polynomial component of the best-fit PFS model. Cyclical phases vary from zero to one, and are defined as the time modulo the best-fit period divided by the best-fit period. Figure 5 shows two complete cycles of the de-trended data, following the method commonly employed by asteroid astronomers.

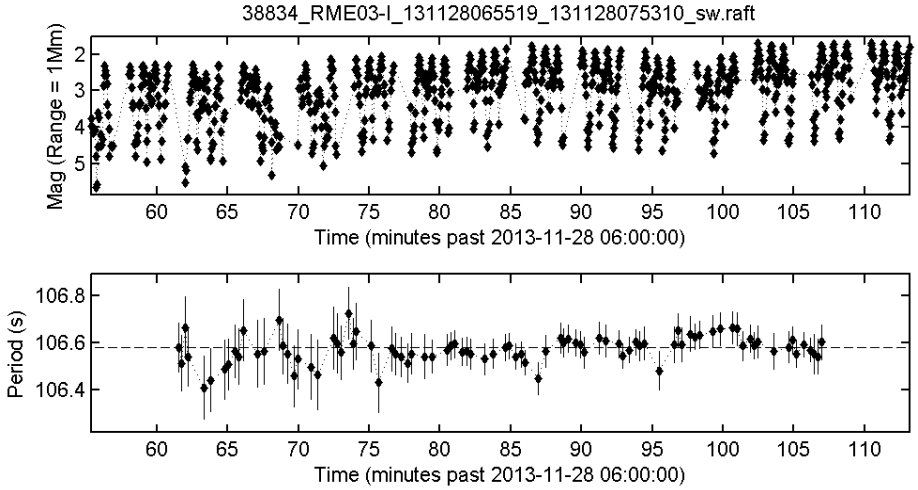

Figure 2. RME Raven telescope light-curve measurement for D4S2 rocket-body SCN 38834 (top panel), and the periods estimated from the data (bottom panel) using the sliding-window periodicity algorithm from [2], which show no statistically significant periodicity variations as a function of time. In this case, performing a synodic/sidereal spin-state analysis would be fruitless.

3.4 Sliding-Window Temporal Analysis to Find Periodicity Variations

The PFS fitting method also provides a means to detect and measure periodicity variations occurring within individual light-curves using a "sliding-window" technique, in which multiple analyses are performed for a series of overlapping windows in time sliding across the light-curve (see [2] for more details). Figures 2-4 show the results

of sliding-window analysis for the D4S2 data, with the input light-curve data plotted in the top-most panel, and estimated periods plotted on the same time scale below. Figure 2 shows an example where no statistically significant periodicity variations are detected (i.e., all of the estimated sliding-window samples are consistent with a flat line). Figure 3 shows an example where weak variations are detected, in this case a modest but detectable downward trend in the periods. Figure 4 shows an example where stronger variations are detected. Specifically, in this long-duration light-curve for SCN 36586, statistically-significant period variations occur between about 11:00 UT and 12:00 UT.

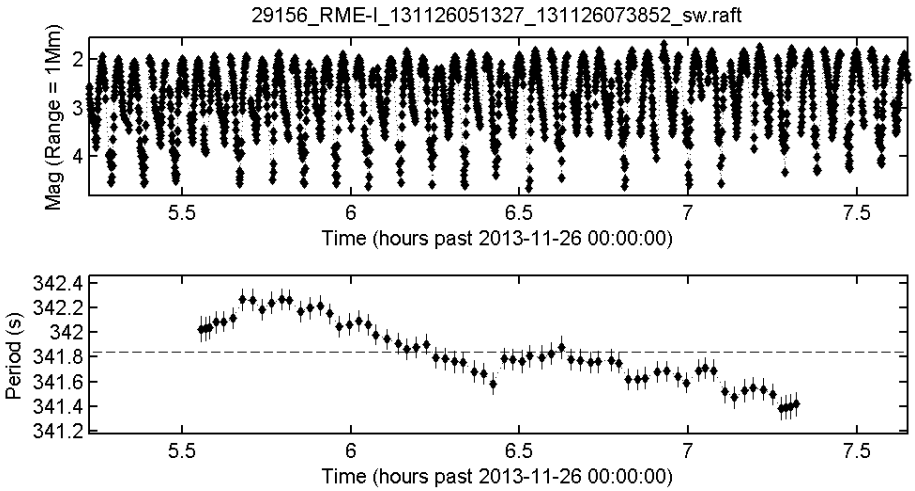

Figure 3. RME Raven telescope light-curve measurement for D4S2 rocket-body SCN 29156 (top panel), and the periods estimated from the data (bottom panel) using the sliding-window periodicity algorithm from reference [2], which shows periodicity variations with a downward trend.

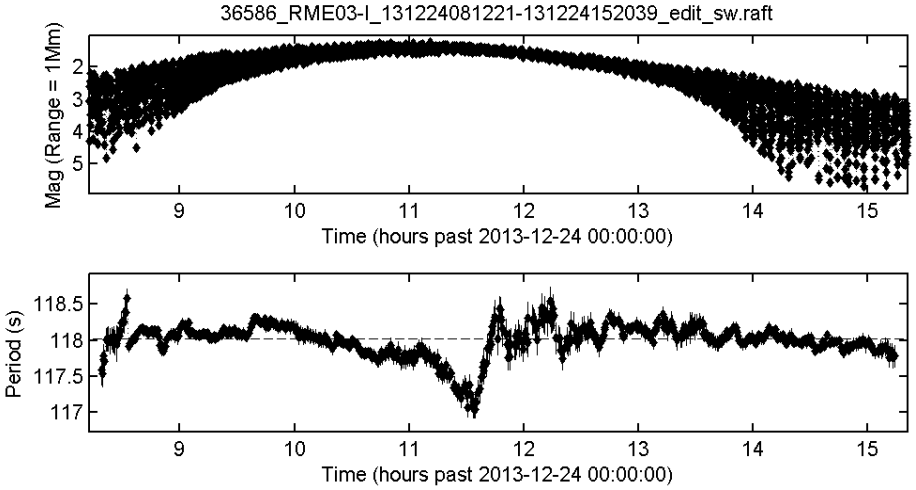

Figure 4. RME Raven telescope light-curve measurement for D4S2 rocket-body SCN 36586 (top panel), the periods estimated from the data (middle panel) using the sliding-window periodicity algorithm from reference [2], which show significant periodicity variations near ~ 11:30 UT.

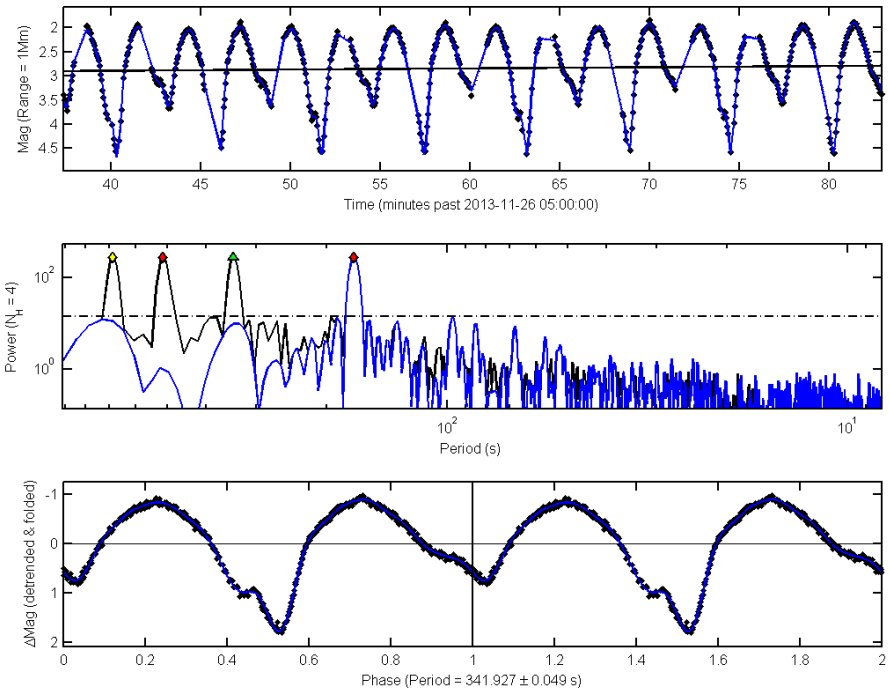

Figure 5. Periodicity analysis for SCN 29156, using the first third of the Raven data plotted in the top panel of Figure 3. The top panel shows the measured light-curve in range-normalized stellar magnitudes (black) and the best-fit Fourier+polynomial series model (blue). The colored symbols in the middle panel show the statistically-significant peaks in the spectrum, and the green triangle marks the best-fit period of 341.927 ± 0.049 s The middle panel shows the raw periodogram frequency spectrum (blue) and the harmonically-extended spectrum (black) [see 2]. The bottom panel shows the de-trended brightnesses (i.e., with the best-fit polynomial model component removed) on the vertical axis, plotted against the cyclical phase (i.e., the time modulo the best-fit period) on the horizontal axis, again with the measurements in black and the best-fit Fourier series model in blue.

4 SHAPE-INDEPENDENT ROTATION-STATE ANALYSIS

Asteroid astronomers have devoted a great deal of effort to develop methods to characterize rotation states using temporal photometry (see [17-19] and references therein) in the absence of *a priori* knowledge of an object's shape. Some of these methods are truly shape independent, in that they do not require knowledge or inference of any object shape or reflectance parameters, while others require that object shape parameters be inferred from the data along with the rotation state parameters.

4.1 Single-Axis Spin States vs. Multi-Axis Rotation States

The first step in a rotation state analysis process entails discriminating complex or multi-axis rotation (precession or precession+nutation) from single-axis rotation (e.g., principal-axis spins). Axisymmetric bodies in multi-axis rotation states produce brightness variations that generally require two frequencies to explain: one for the spinning motion of the body about its principal axis, f_ψ, and another for the precessional "coning" motion, f_ϕ [18, 19]. Generally, axisymmetric bodies in long-axis mode precession states (like many asteroids and most rocket-bodies) produce periodogram spectra with the strongest peak at a frequency of 2 ($f_\psi + f_\phi$). Furthermore, fitting multi-axis rotator light-curve brightness modulations generally requires a two-dimensional Fourier series [18, 19], rather than the one-dimensional Fourier series that is sufficient for single-axis spinners [2]. Fitting 2D Fourier series models to light curves can therefore provide shape-independent means of gaining insight into multi-axis rotation states.

Single-axis spinners, on the other hand, produce light-curves that can be fit to a high level of statistical confidence using a one-dimensional Fourier series. In this regard, finding that a best-fit 1D Fourier series (either alone or supplemented with a polynomial series) fails to sufficiently describe observed light-curve variations can be used as means to infer the existence of multi-axis rotation, without further characterizing the details of the rotation state. This eliminates the need to calculate a more computationally-intensive 2D Fourier series fit, or the much more intensive analysis to estimate other rotational parameters (e.g., the angular momentum vector or the object's moment-of-inertia ratios) that also generally require a simultaneous shape analysis [19].

4.2 Synodic/Sidereal Spin State Analysis

Satellite spin states can be further characterized by first detecting and then analyzing synodic/sidereal variations, as described in detail in reference [2]. Synodic periods are the apparent period measured from the light-curves, and can be influenced by the relative motion of the satellite, observer, and illumination source. For instance, if a spinning body moves quickly with respect to an observer, the apparent rotation rate *as seen from the observer's perspective* can deviate significantly from the actual rotation rate of the body. (An extreme example in this respect is the Moon, which always presents the same face to the Earth showing *a synodic rotation rate of zero* even though it actually has a sidereal rotation rate of 1 revolution every 28 days.) Although developed for asteroid characterization, the synodic/sidereal method applies equally well to artificial satellite observations because it is independent of the shape and reflectance characteristics of the observed object. In fact, the sliding window PFS periodicity analysis described in section 3.4 was designed specifically to detect synodic periodicity variations [2].

The synodic/sidereal method uses a set of measured synodic frequencies to estimate a rotating object's sidereal angular spin rate and spin axis orientation. This method relies on two fundamental assumptions: 1) that the observed body is in a stable spin rotation state, and 2) that each full-cycle synodic period measured by the observer corresponds to the time interval required for the body to rotate such that the "phase angle bisector" (PAB) makes one complete revolution in azimuthal angle around the spin axis. The PAB is the direction midway between the body-to-observer and body-to-Sun direction vectors. Over short time scales, corresponding to small changes in observation and solar illumination angles, the single-cycle reflected-light signature of a spinning body is controlled to a large extent (but not entirely) by the position of the PAB in the body's reference frame. This provides the basis for the second assumption, and makes the method shape-independent to first order.

Synodic/sidereal spin state estimation analyses can be performed using the algorithm described in reference [2]. In that case, the results were shown using a least-squared chi-squared metric plotted over the unit sphere using a Mollweide projection (see Figure 7 of [2]). The current analysis uses a similar algorithm to estimate a set of three parameters, $\{\theta_0, \psi_0, \omega\}$, which denote the two Euler angles of the spin axis, and the sidereal angular spin rate $\omega = d\psi/dt = 2\pi/T$, where T is the sidereal full-cycle period. The two Euler angles convert directly to the inertial spin axis RA/DEC angles, $\alpha_0 = \phi_0 - \pi/2$ and $\delta_0 = \pi/2 - \theta_0$, respectively. The current algorithm also provides an estimate for the probability distribution function (PDF) of the spin axis orientation. Ideally, this PDF has a single sharp maximum, indicating that the estimation process has converged to a single a single, well-determined spin axis. This is indeed the case when the current method is applied to the IMAGE satellite data from [2], which contain strong, well-detected synodic periodicity variations. However, in cases where synodic variations are less strongly detected, the PDF can have multiple local maxima and/or be widely distributed, indicating either multiple feasible solutions and/or large extended regions where feasible solutions exist. In these cases, improving the spin state estimate entails acquiring light-curve data that show stronger and/or better-detected synodic variations.

4.3 Synodic/Sidereal Spin State Analysis for Delta-IV Stage 2 Rocket- Body SCN 38834

The lower panel of Figure 2 shows that, in this SCN 38834 data set, no synodic variations were detectable using the sliding window method. Notably, this does not mean that none exist, just that none were detectable at a sufficient level of confidence. This really means that a flat line fits the period measurements along with their error bars, which is clearly the case shown in the in the middle panel plot of Figure 2. Synodic variations at a level smaller than the 1-sigma error bars could (and probably do) exist, but cannot be detected in the given data set. Notably, these error bars can be reduced by temporal measurements with higher SNR, faster cadence, and/or longer light-curve duration, which points to the most natural means of increasing probabilities of synodic detections for this object. However, given that this this data set contains no detectable synodic variations, then no synodic/sidereal spin state analysis can be performed, and the spin axis cannot be constrained at all.

4.4 Synodic/Sidereal Spin State Analysis for Delta-IV Stage 2 Rocket- Body SCN 29156

The lower panel of Figure 3 shows an example where weak synodic variations have been detected for SCN 29156, which, in turn, allows a synodic/sidereal spin state estimation analysis to be performed. Figure 6 shows the resulting PDF of the spin axis orientation using a Mollweide projection. Notably, in this case the PDF is non-zero over a large region of the unit sphere has four local maxima, indicating multiple feasible solutions — a direct result of the weakly detected synodic variations.

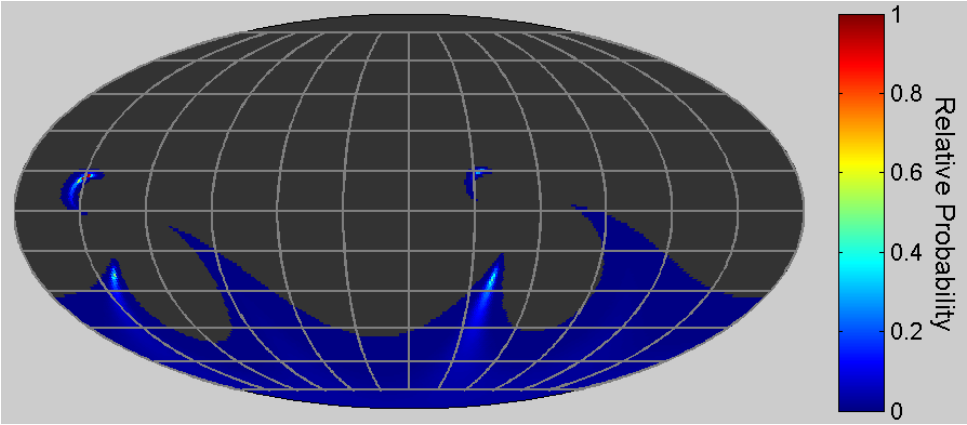

Figure 6. The probability distribution function of the spin axis resulting from synodic/sidereal analysis of the synodic periodicities for SCN 29156 plotted in the lower panel of Figure 3. The widely distributed, multi-peaked PDF indicates that the estimation process yielded multiple feasible spin-state solutions. In this case, higher-quality data must be gathered to converge on an isolated, unique solution.

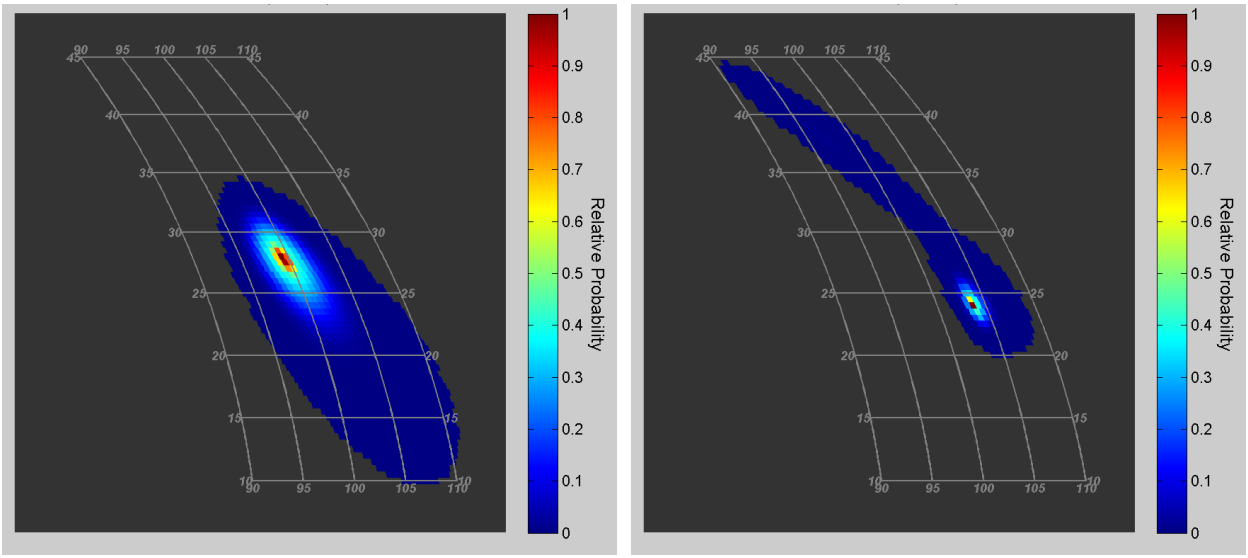

Figure 7. The probability distribution functions of the spin axis resulting from two different estimation analyses for the D4S2 rocket-body SCN 36586, both based on the light-curve data shown in Figure 4. The left panel shows the PDF from the shape-independent, synodic/sidereal method, and the right panel from the shape-dependent, simple-cylinder-approximation rotation state analysis. Note that both PDFs are plotted on the same scale, and the grid lines indicate RA and DEC values in the horizontal and vertical directions respectively. These sharply-peaked PDFs indicate both methods converge on well-determined solutions, although with somewhat different overall shapes and peak RA/DEC values.

4.5 Synodic/Sidereal Spin State Analysis for Delta-IV Stage 2 Rocket- Body SCN 36586

The lower panel of Figure 4 shows an example where stronger synodic variations have been detected. Specifically, for that SCN 36586 2013-12-24 light-curve, the sliding-window method detects relatively strong periodicity variations in the hour or so centered at ~ 11:30 UT. Subjecting these variations to a synodic/sidereal analysis yields the spin axis PDF shown on the left panel of Figure 7. Notably, this PDF has a relatively sharp peak, and the figure shows a Mollweide projection of just a portion of the unit sphere centered on the peak. The best-estimate spin state in this case has a sidereial period of T = 118.2689 ± 0.0051 s, a spin axis orientation given by J2000 right-ascension and declination α_0 = 99.4° and δ_0 = 27.8°, with a 1-sigma estimation uncertainty of about 1.1°.

5 SHAPE-DEPENDENT ROTATION-STATE ANALYSIS

The periodicity-based methods described in the previous section provide rotation state information in a shape-independent fashion, i.e., without any explicit consideration of the object's shape or reflectance characteristics. Alternatively, shape-dependent rotation state estimation processes can be formulated. These come in three basic categories: 1) those in which *all* shape/reflectance information is estimated from the data along with the rotation state information), 2), those where *some but not all* of the shape/reflectance information is estimated, or 3) those where *no* shape/reflectance information is estimated (because it is all known or assumed *a priori*). Most shape-dependent asteroid methods fall into the second, hybrid category (see [17-19] and references therein), because these methods usually assume some *a priori* knowledge of the asteroid surface bi-directional reflectance distribution function (BRDF), and then estimate the asteroid's shape via a best-fit parameterized model. This hybrid approach can be used because asteroid BRDFs are relatively well studied, but their shapes are generally unknown [17]. Asteroid shape models range considerably in complexity: from simple (tri-axial ellipsoids), moderate (spherical-harmonic surface expansion, multi-vertex convex-hulls), up to relatively complex (multi-vertex surfaces with concavities).

5.1 Rotation State Estimation for Satellites of Known Shape and Reflectance

For man-made satellites with known shapes and materials, one may be tempted to evaluate rotation states using the third method discussed above, in which no shape/reflectance information about the object is estimated in the analysis process. This estimation process requires having a complete model of the shape and reflectance characteristics of a satellite, and then using a forward-modeling process such as that described in [20] in order to estimate only the object's attitude parameters, an approach used in [21] for stabilized satellites and [22] for satellites that have potentially maneuvering attitudes. For objects in torque-free multi-axis rotation states, this kind of analysis would entail estimating the following set of eight parameters [18, 19]: $\{\phi_0, \theta_0, \psi_0, \mathbf{L}, i_1, i_2\}$. Here $(\phi_0, \theta_0, \psi_0)$ denote the body's orientation Euler angles for a given initial time, t_0, $\mathbf{L}$ is the 3-component angular momentum vector, and (i_1, i_2) are the two smallest principal-axis-frame moments of inertia, normalized to the largest moment of inertial (i.e., $i_1 = I_1/I_3$, and $i_1 = I_2/I_3$). In this case the rotation state estimation process entails solving an eight-dimensional optimization problem [19]. However, this dimensionality can be reduced by one for bodies with axi-symmetric mass distributions because $i_1 = i_2$, a good approximation for many asteroids [17] and man-made rocket-bodies [23]. Furthermore, for objects in torque-free principal-axis spin states, the equations of motion no longer depend on (i_1, i_2), and the set of estimated parameters can be reduced to four, $\{\phi_0, \theta_0, \psi_0, \omega\}$, where, as before, the first two Euler angles provide the spin axis orientation and ω denotes the angular spin rate.

The rotation state parameters outlined above strictly apply to objects in torque-free environments. However, satellites in Earth orbit are perturbed by environmental torques [e.g., 23]. In this case, the parameters outlined above would still apply, but must be estimated from light-curve data collected over a time-scale sufficiently short so that perturbations from on-orbit torques can be safely neglected.

5.2 Rotation State Estimation for Objects of Unknown Shape and Unknown Reflectance Characteristics

Reference [24] outlines an attitude evaluation method requiring no *a priori* shape or reflectance information (also see [25]). In this case, the surface of the man-made satellite being observed is modeled as an ensemble of flat facets, and the size and reflective properties of each facet estimated from the light-curve data along with the rotation state parameters. The sizes of the facets can be modeled in terms of albedo-area products [24] or as projected areas [25]. Different surface compositions on the satellite's surfaces can be accounted for by estimating different specular vs. diffuse components for individual facets [24], adjusted to match shiny vs. dull materials. This approach has the advantage of being applicable to completely unknown satellites, but increases the dimensionality of the optimization analysis considerably, sometimes to a computationally-prohibitive extent.

5.3 Rotation State Estimation for Objects of Known Shape but Unknown Reflectance Characteristics

Often satellites have known shapes, but the materials covering their surfaces are unknown or have uncharacterized reflectance characteristics. In these cases, a hybrid approach is possible where only the surface BRDF parameters are estimated along with the rotation state parameters. These BRDF parameters could comprise laboratory-measured material reflectance functions, in which case the process would entail estimating which materials on which satellite surfaces (or components) provide the best match to the observed data, which might be formulated in a manner similar to that described in [26], or as a linear-programming or discrete goal-maximization optimization analysis. Alternatively, the parameters could comprise a set of analytical BRDF expansion functions such as those described in [27], which would naturally adjust to match surface material shiny vs. dull reflectance properties, which is the approach used in this analysis. The known shapes could comprise wireframe models or solid models for

complex satellites, or more basic shapes to approximate simpler objects (e.g., cubes or for CubeSats, cylinders for rocket-bodies, etc.).

5.4 Rotation State Estimation for Nearly Cylindrical Objects

Some satellites can be approximated reasonably well using simple cylindrical shapes to model reflected brightnesses. These include Boeing 376 GEO satellites — dual-spinning cylindrical satellites with outer round surface covered in shiny solar cells — which can produce bright, short-duration flashes when they glint sunlight [1, 4]. Because the timing of the bright flashes can be measured very accurately, synodic periodicity variations for these objects can be tracked much better than for less shiny objects.

Upper-stage rocket-bodies can also be approximated as cylinders, although perhaps less accurately than Boeing 376 satellites. Figure 1 shows that the D4S2 rocket-bodies do have a roughly cylindrical shape, and much of their projected area comprises a nearly perfectly cylindrical white-colored surface. Our observations indicate that the specular component of reflection for D4S2s is very low, which means that they generally do not produce bright, short-duration flashes. This is demonstrated in the bottom panel of Figure 5, which shows an observed D4S2 rotational light-curve characterized by the two-peaks-per-cycle brightness pattern expected for a cylinder in principal axis rotation [28]. Notably these brightness peaks are not short, bright spikes, as is observed for Boeing 376 satellites [1, 4]. Because of this, non-specular rocket-bodies such as D4S2s do not lend themselves as readily to synodic/sidereal spin state analyses. This is especially true for rocket-bodies in orbits that have high perigee altitudes (e.g., GPS D4S2s), that move at very low-angular rates relative to ground-based observers, which also makes synodic periodicity variations more difficult to detect [2]. In fact, multiple Raven light-curve observations of the D4S2s that have launched GPS satellites have been conducted, and most yield no detection of synodic variations (as shown in the bottom panel of Figure 2) or only weak detections (Figure 3, bottom panel). In fact, the synodic variations shown in the bottom panel of Figure 4 represent the strongest detected in about a dozen D4S2 light-curves of comparable quality. Our analysis indicates that those variations were likely detected only because during that light-curve the PAB vector made a relatively close approach to the spin axis, an effect which tends to create large synodic variations [1, 2].

These difficulties of measuring synodic variations for non-specular rocket-bodies prompt an investigation of a shape-dependent spin-state estimation process. For this, brightnesses are approximated using a simple cylinder shape model, characterized by flat top and bottom surfaces with pure Lambertian reflectances, and a round surface with Lambertian + specular reflectances. Each surface is parameterized using albedo-area (aA) products (see [24, 25]). The top and bottom surfaces are parameterized by (aA_T, aA_B). The round surface is parameterized by a Lambertian albedo-area product, aA_S, as well as a series of specular functions aA_m, where the index m spans a range of specular functions such as a series of Phong or Cook-Torrance BRDFs (see [24] for more details and examples). These aA products must be estimated along with the rotation state parameters using a process that seeks the best fit to the observed light-curve data.

5.5 Spin State Estimation for Delta-IV Stage 2 Rocket-bodies

For this study we've developed and implemented a shape-dependent algorithm to estimate spin states using the simple-cylinder formulation outlined above. Our analysis of multiple D4S2 data sets indicates that adding specular components to the shape model does not improve the quality of the fits to the light-curves in a statistically justifiable way. So for D4S2s, seven parameters must be estimated for the shape-dependent spin state analysis: $\{\phi_0, \theta_0, \psi_0, \omega, aA_T, aA_B, aA_S\}$. While still numerically tractable, this is significantly larger than the three required for the shape-independent synodic/sidereal analysis, $\{\phi_0, \theta_0, \omega\}$, as described in section 4.2. Space limitations prevent a detailed description of our newly-implemented shape-dependent formulation in this paper, but a few salient features based on analyses of simulated rocket-body data sets warrant comment:

1. The seven-dimensional parameter space for the estimation process is characterized by highly non-linear objective functions with multiple local extrema (some cyclical in nature), so confidently finding a global solution to the optimization problem can be exceedingly computationally intensive.
2. The search range for the spin rate ω should be limited to a realistic span provided by a previously-calculated periodicity analysis, allowing for some reduction of computation.
3. Given a hypothesized spin state $\{\phi_0, \theta_0, \psi_0, \omega\}$, best estimates for the aA products can be found in a straightforward manner [2], also providing a means to reduce computation.
4. Employing data with phase angles greater than about 60° to 90° can lead to both biases and inaccuracies in the estimation process, apparently because the simple-cylinder shape model approximation fails to match both high- and low-phase-angle data simultaneously.

5. Our current analytical formulation for uncertainties and covariances tends to significantly underestimate deviations from known truth for the simulated rocket-body analyses. This also may be due to the oversimplified shape model, but warrants further study. Numerical boot-strap or jack-knife uncertainty estimates would likely provide better agreement, but are computationally intensive and have not been implemented for this study.
6. Although the shape-dependent formulation does not require that synodic variations be present in the input data, it turns out that when none exist, the analysis generally provides two equal-quality, degenerate spin state solutions with oppositely-directed spin axis orientations. In other words, the shape-dependent method has difficultly discriminating between clockwise and counter-clockwise spins. This result is not surprising, and can be predicted from simple symmetry considerations. However, given light-curves that do include strong synodic variations, a properly formulated shape-dependent estimation analysis should be able to converge to a unique spin axis, just like the synodic/sidereal method does.

The right panel of Figure 7 shows the spin axis PDF calculated by applying the shape-dependent estimation process describe above to the D4S2 SCN 36586 2013-12-24 light-curve shown in the top panel of Figure 4, but restricted to phase angles ≤ 70° to limit bias and inaccuracies. Note that this shape-dependent PDF is plotted on the exact same scale as the shape-independent PDF shown in the left panel, and is based on the same data set. The shape-dependent analysis also yields a PDF with a relatively sharp peak, but a somewhat different best-estimate spin state: sidereal period T = 118.2940 ± 0.0036 s, and spin axis J2000 RA/DEC values α_0 = 103.8° and δ_0 = 24.0°, with a analytically-estimated 1-sigma estimation uncertainty of about 0.2°. These parameters agree reasonably well with the synodic/sidereal values (reported in section 4.5): the sidereal periods only differ by ~ 0.025 s and the spin axis unit vectors by ~ 5.5°. However, these differences significantly exceed the estimated 1-sigma ranges for both methods, which we believe to be due (at least in part) to systematic under-estimation of uncertainties that the shape-dependent analysis provides (at least in its current formulation). The process also yields aA estimates of ≤ 1.5 m^2 for the two cylinder ends and ~ 42 m^2 for the round side, consistent with the known dimensions and materials for D4S2 rocket-bodies.

It is also worth noting that calculating the shape-dependent PDF shown on the right panel of Figure 7 required approximately a factor of 100 more computation time than the shape-independent synodic/sidereal PDF on the left panel. This difference arises because the shape-dependent analysis has significantly higher dimensionality and non-linearity than the shape-independent approach. It is likely that for more complicated satellites, this computational difference will be even more dramatic — because those objects will require higher dimensionality shape models than the simple cylinder employed here — probably requiring the use of parallel, multi-node computing.

6 CONCLUSIONS AND FUTURE WORK

Our study of D4S2 rocket-bodies satellites indicate that synodic variations can be difficult to detect from the ground for these non-specular, nearly-cylindrical objects. Multiple Raven D4S2 light-curve observations were conducted for this study, with most yielding none or weak synodic detections. Only one light-curve provided relatively strong synodic variations, for SCN 36586 as shown in Figure 4. Spin state analyses of this light-curve using the shape-independent synodic/sidereal approach as well as a shape-dependent simple-cylinder approach yield roughly the same results for the object's spin state parameters — although significantly outside the estimated 1-sigma limits of one another, which warrants more investigation. So our analysis indicates that a simple-cylinder shape model can, in principle, suffice to characterize rotation states for upper-stage rocket bodies observed at low phase angles, although more work needs to be accomplished.

Overall, the difficulty in detecting synodic variations from the ground for objects in high-altitude orbits compels an investigation of shape-dependent spin state analysis methods, which do not require detection of synodic variations. Unfortunately, shape-dependent approaches seem be relatively computationally intensive, and often yield two degenerate solutions with oppositely-directed spin axes. For these reasons, the shape-independent synodic/sidereal spin-state estimation approach should be favored whenever feasible, which sometimes entails acquiring light-curve data that show stronger and/or better-detected synodic variations. In this regard, it is worth noting that even for deep-space objects, one can significantly improve the detectability of synodic variations even for non-specular objects by using a space-based sensor [29].

7 REFERENCES

1. Lambert, J., et al., "Observations of Retired Boeing 376 Spacecraft", *The 2003 AMOS Technical Conference Proceedings*, Kihei, HI, 2003.
2. Hall, D., et al., "AMOS Observations of NASA's IMAGE Satellite", *The 2006 AMOS Technical Conference Proceedings*, Kihei, HI, 2006.

3. Wallach, B., Somers, P. and Scott, R., "Determination of Spin Axis Orientation of Geosynchronous Objects using Space-Based Sensors: An Initial Feasibility Investigation", *The 2010 AMOS Technical Conference Proceedings*, Kihei, HI, 2010.
4. Somers, P. "Cylindrical RSO Signatures, Spin Axis Orientation and Rotation Period Determination", *The 2011 AMOS Technical Conference Proceedings*, Kihei, HI, 2011.
5. Hall, D. "AMOS Galaxy 15 Satellite Observations and Analysis", *The 2011 AMOS Technical Conference Proceedings*, Kihei, HI, 2011.
6. Payne, T. et al., "SSA Analysis of GEO Photometric Signature Classifications and Solar Panel Offsets", *The 2006 AMOS Technical Conference Proceedings*, Kihei, HI, 2006.
7. Gregory, S., et al., "Comparison Between TASAT Simulations and Color Photometry Observations of GEOs", *The 2008 AMOS Technical Conference Proceedings*, Kihei, HI, 2008.
8. Payne, T. et al., "Signature Intensity Derivative and its Application to Resident Space Object Typing", *The 2009 AMOS Technical Conference Proceedings*, Kihei, HI, 2009.
9. Vrba, F., et al., "A Survey of Geosynchronous Satellite Glints", *The 2009 AMOS Technical Conference Proceedings*, Kihei, HI, 2009.
10. Murray-Krezan, J., et al., "Algorithms for Automated Characterization of Three Axis Stabilized GEOs Using Non-resolved Optical Observations", *The 2012 AMOS Technical Conference Proceedings*, Kihei, HI, 2012.
11. United Launch Alliance, "Delta IV Payload Planners Guide", *ULA P.O. Box 277005, Littleton, CO, USA, 80127*, 2007.
12. Space-Track.org Website, www.space-track.org, as of July 03, 2014.
13. Africano, J., et al., "AMOS Debris Observations", *Proc. of the Third European Conference on Space Debris, Darmstadt*, Germany, 19-21 March, 2001.
14. Sabol, C., et al., "Recent Developments of the Raven Small Telescope Program", *AAS/AIAA Space Flight Mechanics Meeting*, AAS 02-131:397, 2001.
15. Scargle, J., "Studies in Astronomical Time Series Analysis II. Statistical Aspects of Spectral Analysis of Unevenly Spaced Data," *The Astrophysical Journal*, Vol. 263, 834–53, 1982.
16. Press, W. et al., "Numerical Recipes in FORTRAN: The Art of Scientific Computing" (2nd Edition), Cambridge University Press, New York, NY, 1992.
17. Magnusson, P. et al., "Determination of Pole Orientations and Shapes of Asteroids," in *Asteroids II* (edited by R. Binzel et al.) 66–97, University of Arizona Press, 1989.
18. Kaasalainin, M., "Interpretation of Lightcurves of Precessing Asteroids", A&A, Vol 376, pp. 302-309, 2001.
19. Pravec, P., et al., "Tumbling Asteroids", *Icarus*, Vol. 173, pp. 108-131, 2005.
20. Riker, J., and Butts, R., "The Time-Domain Analysis Simulation for Advanced Tracking (TASAT) Approaches to Compensated Imaging", SPIE Vol.1688, *Atmospheric Propagation and Remote Sensing*, 1992.
21. Nishimoto, D., et al., "Satellite Attitude from a Raven Class Telescope", *The 2010 AMOS Technical Conference Proceedings*, Kihei, HI, 2010.
22. Holzinger, M. J., et al., "Attitude Estimation for Unresolved Agile Space Objects with Shape Model Uncertainty", The *2012 AMOS Technical Conference Proceedings*, Wailea, Maui, Hawaii, 2012.
23. Ojakangas, G. W. and Cowarding, H., "Probable Rotation States for Rocket-Bodies in Low-Earth Orbit", *The 2013 AMOS Technical Conference Proceedings*, Kihei, HI, 2013.
24. Hall, D. "Separating Attitude and Shape Effects for Non-resolved Objects", *The 2007 AMOS Technical Conference Proceedings*, Kihei, HI, 2007.
25. Calef, B., et. al., "Photometric Signature Inversion" in "Unconventional Imaging II" ed. Gamiz, V., *Proceedings of SPIE*, Vol. 6307, 63070E, 2006.
26. Hall, D., "Surface Material Characterization from Multi-band Optical Observations", *2010 AMOS Technical Conference*, Wailea, Maui, Hawaii, 2010.
27. Hall, D., "Surface Material Characterization from Non-resolved Multi-band Optical Observations", *2012 AMOS Technical Conference*, Wailea, Maui, Hawaii, 2012.
28. Cowardin, H., et al., "Optical Signature Analysis of Tumbling Rocket Bodies via Laboratory Measurements", *2012 AMOS Technical Conference*, Wailea, Maui, Hawaii, 2012.
29. Wallace, B., Somers, P., and Scott, R. L., "Determination of Spin Axis Orientation of Geosynchronous Objects Using Space-Based Sensors: An Initial Feasibility Investigation", *2010 AMOS Technical Conference*, Wailea, Maui, Hawaii, 2010.